CONSIDERATIONS ON ACTIVE REDUCTION NOISE, TREATMENT AND CONTROL DESIGN PERFORMANCE AT DIESEL GENERATOR

CRISTIANA VOICAN[1], C.D. STĂNESCU [2]

Abstract. This paper discusses the methodology and results of a noise audit and active control testing on a portable single-cylinder diesel generator. Using a large microphone array, a spectral intensity map of all external surfaces of the generator set was constructed from experimental measurements. Two primary noise sources were measured: a relatively directional high-frequency structurally-coupled engine component, and low-frequency fundamental exhaust firing-order harmonics. The low-frequencies were reduced using the feed-forward Filtered-X LMS with a reference derived directly from the electrical generator coupled to the diesel engine.

Key words: noise, audit, diesel, generator, frequency.

1. INTRODUCTION

Portable generators are a necessity for many industrial, personal and military applications. Unfortunately, using an internal combustion engine to generate electricity produces unwanted noise in addition to the desired electrical power. The reduction of the noise produced by these machines is often done as an afterthought to the original design. For the investigation of this paper, a noise audit and active/passive treatment was performed on a 3 kW single-cylinder diesel generator. The generator set already had noise treatments applied by encasing it in an alluminum enclosure, with passive poro elastic treatments on the panels and on all inlets and outlets.

Fig. 1 – 3 kW generator with example prototype ANC source.

[1] Technical College of Bucharest, Romania; *E-mail*: voicancristiana@yahoo.com)

[2] "Politehnica" University of Bucharest, Romania; *E-mail*: prof cstanescu@yahoo.com)

Rev. Roum. Sci. Techn. – Méc. Appl., Tome 56, Nº 2, P. 141–151, Bucarest, 2011

2. NOISE SOURCE AUDIT AND MESSUREMENT PROCEDURE

The microphone phased array shown in Fig. 2 was used to map the generator enclosure radiation noise sources. The inside and outside diameters of the array were 9.8 inches and 59.8 inches, respectively. The array center body was provided with a laser pointer that projects a laser dot along a line perpendicular to the array plane passing through the center of the array. Phased-array measurements were carried out from four positions relative to the generator. The array was successively placed at 128 inches from each side panel of the generator such that the laser was pointing to the center of the top edge of the panel.

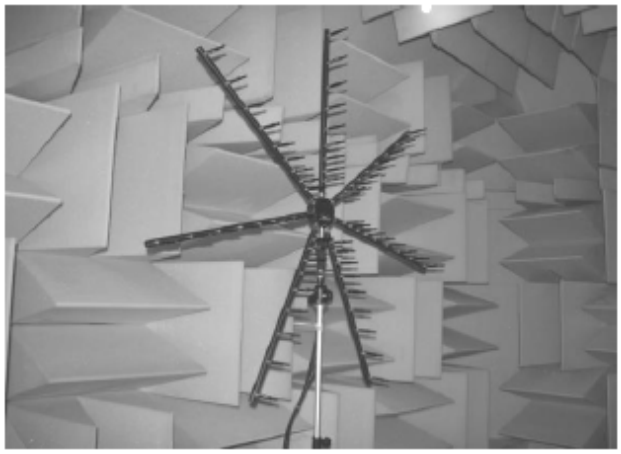

Fig. 2 – The 63-element microphone phased-array.

The 63 microphone signals were sampled simultaneously at 51 200 samples per second in 25 separate blocks of 16 384 samples each. Time-domain data was processed using a frequency domain, phased-array, beamforming code developed at Virginia Tech. Diagonal removal was used in the post-processing of the phased-array data to minimize the effects of uncorrelated background noise. For each array position, the data was processed over a scanning plane that contained the panel the array was facing, with a 1-inch resolution in both horizontal and vertical directions.

Results were obtained in the form of narrow band acoustic maps in the range of 1 200 to 1 500 Hz. The four side panels measured by the array are labeled as shown in Table 1.

Table 1

Panels measured by the array

Face 1	Operator panel	27" × 26" (W × H)
Face 2	Access panel	34" × 26"
Face 3	Opposite operator panel	27" × 26"
Face 4	Exhaust panel	34" × 26"

3. HIGH FREQUENCY RESULTS

Figure 3 shows the average microphone spectrum for the array positioned in front of face 2. This figure helped to identify specifying frequency ranges to choose for plotting the beamforming maps. For example, the figure indicates that a large part of the high-frequency spectral energy is contained in the frequency range of 1 200–1 500 Hz, with a dominant peak around 1 400 Hz. This frequency band was chosen to identify the noise sources on the side-panel surfaces.

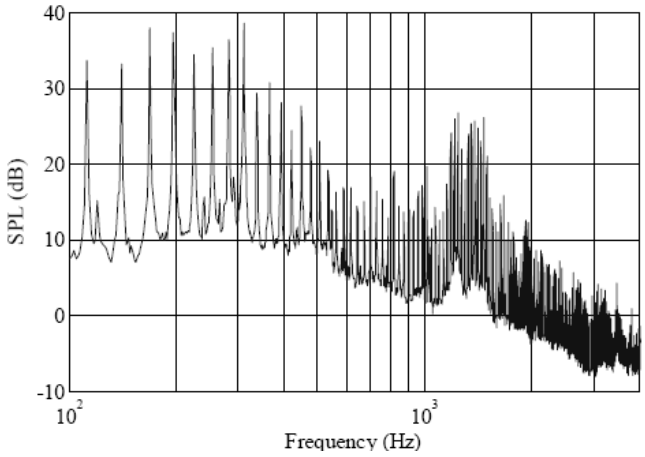

Fig. 3 – Average microphone spectrum for the array in front of face 2.

Figures 4a–4d show the beamforming maps of the generator noise for the array positioned in front of faces 1 to 4, respectively. The sound pressure level (SPL) in these plots is uncalibrated but this is unimportant as only the relative sound levels are necessary to identify the noise sources.

In Fig. 4a, a strong radiation component is observed below the generator enclosure, which can be explained by the presence of drainage holes on the bottom pan of the structure. The bottom pan is not resting directly on the ground, but is lifted by about 4 inches due to the presence of forklift skids. Noise radiating from these holes thus reflects off the ground and contributes largely to the 1 400 Hz tones. Fig. 4c shows similar results for the opposite panel (face3).

In Fig. 4b (face 2), most of the noise is emitted from the top of the enclosure, where the fan exhaust, the fan intake and the engine exhaust are located. The sources, together with the radiation of the top panel, are likely causes of the sound pattern observed.

In Fig. 4d (face 4), the major contribution is located in the left half of the panel surface, indicating that this particular part of the structure is radiating considerably within the frequency range of interest. The engine muffer is behind this panel and is likely exciting it acoustically from within.

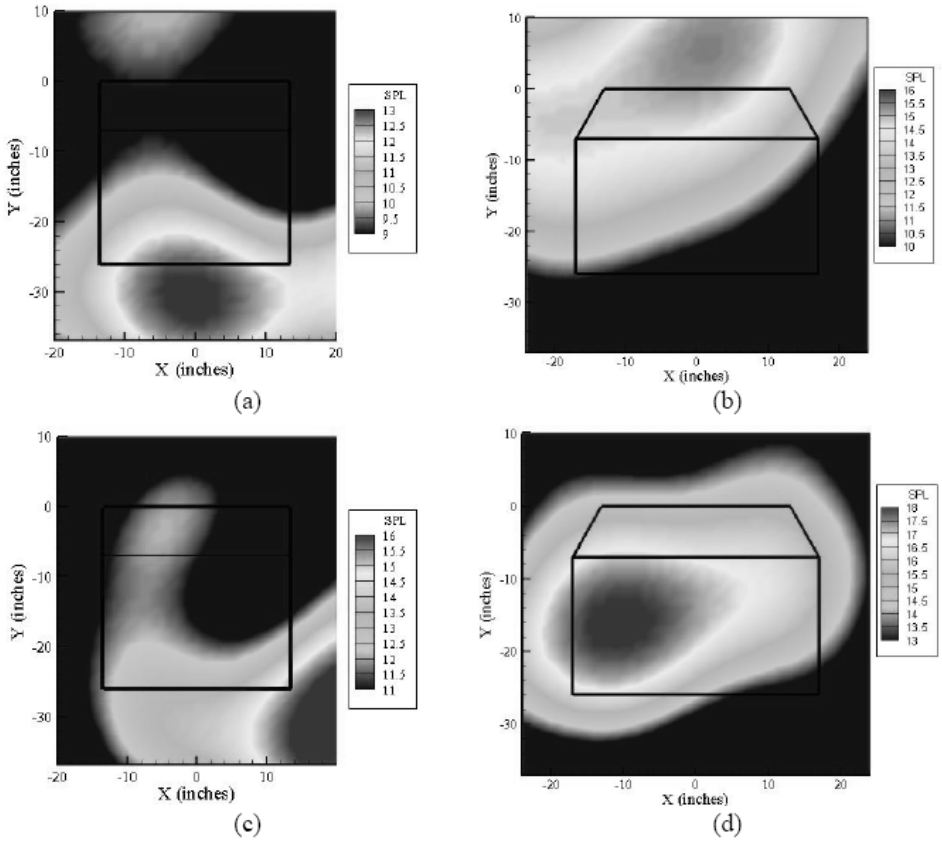

Fig. 4 – Beamforming maps of: a) face 1 at 1 394 Hz; b) face 2 at 1 380 Hz; c) face 3 at 1 411 Hz and d) face 4 at 1 412 Hz. The shape of the compressor is outlined in black solid line.

Several parts of the enclosure are contributing to the 1 400 Hz tones, by emitting both structure-borne and air-borne noise. However, the dominant SPL zones on Fig. 4 are just a few decibels above the average SPL. Thus, even if the dominant sources are eliminated, secondary sources will still add up to produce significant acoustic power. Therefore, an effective passive noise control strategy has to both reduce local dominant sources and provide a global treatment. Based on these considerations and on the observations made from the beamforming maps, the following additional passive noise control treatments were added to the enclosure:

a) Ribs made of ½ inch angle aluminum were attached to face 3 and face 4, in order to add stiffness locally. This would reduce the 1 400 Hz radiation shown prominently in Fig. 4c,d;

b) The absorptive materials from the air inlet and outlet ducts on face 3 was removed, replaced and repositioned for better noise control. The standard material was also augmented with additional absorptive material. Care was taken to keep

the cross sectional areas of the inlet and outlet duct the same size, in order to maintain the same air cooling flow.

c) Absorptive material was added to the inside of the enclosure particularly on the operator panel side. Care was taken to taken to add a minimum of material and not impede access or operation/cooling of mechanical components.

d) Acoustic material was located in the skid access slots under the machine on the region of the drainage holes discussed above.

4. LOW FREQUENCY MEASUREMENT RESULTS

In addition to the phased-array maps, the coherence between the far field sound levels to both structural and acoustic sources was measured. An accelerometer was placed on the cylinder head of the diesel engine and the coherence between it and a far-field microphone was measured as in Fig. 5. As it can be seen, a number of harmonics below 400 Hz show reasonably good coherence, which would allow for good active noise control.

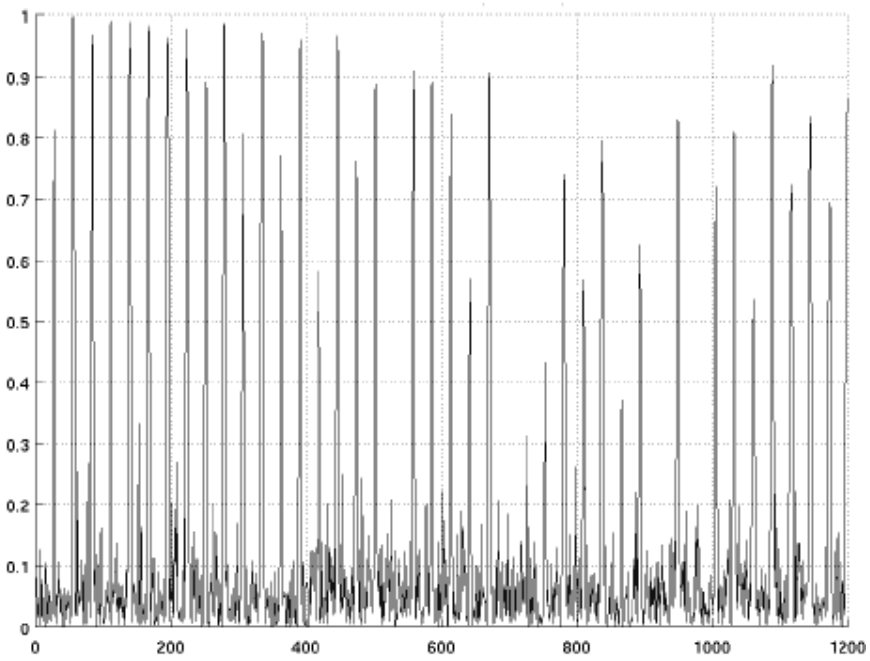

Fig. 5 – Coherence between far field microphone and accelerometer on cylinder head.

Together with structurally-borne sound, the exhaust pulsations were a likely contributor to farfield, low-frequency sound. The coherence of this acoustic signal to the far-field microphone can be seen in Fig. 6.

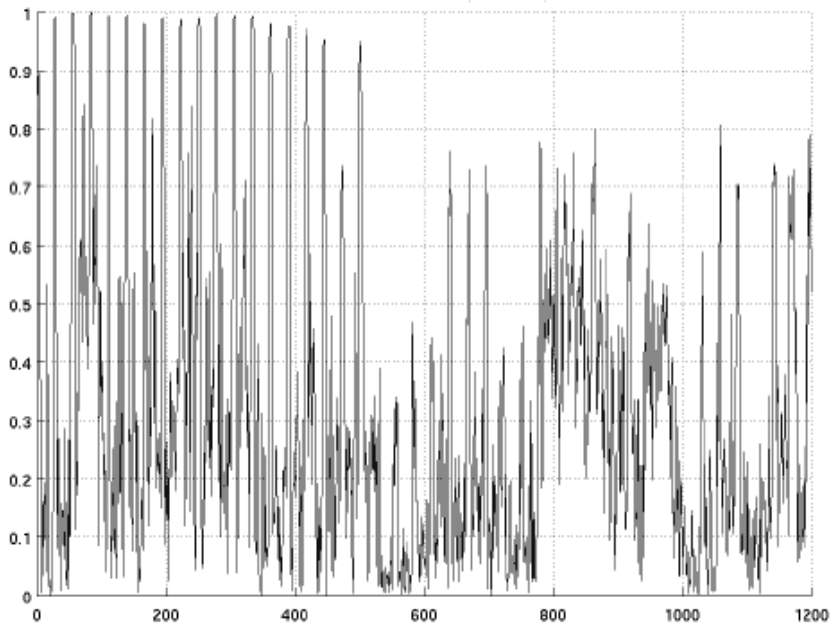

Fig. 6 – Coherence between far field microphone located near exhaust outlet.

5. REFERENCE GENERATION

The electrical side of the generator used for this experimental setup consisted of a synchronous permanent magnet machine coupled to a dedicated full-time inverter. This configuration allows for decoupling of the engine speed to the required synchronous electrical frequency of either 60 Hz or 400 Hz. It also allows for a high-efficiency permanent magnet machine to be used without requiring field adjustment for maintaining the correct output voltage. In addition to the main windings, the machine also had a small, lower-voltage single-phase winding used to charge the engine's starting battery. This winding provided the necessary phase-locked reference to the engine rotation at a lower voltage than using one of the main windings. The electrical frequency of the winding is given by the following relationship:

$$f = \frac{\mathrm{RPM} \times N_{\mathrm{poles}}}{120} \ .$$

However, the 4-cycle engine only fires every 720 degrees of rotation. From the number of poles on the machine, the integer ratio between the firing of the machine and the electrical frequency was calculated.

The circuit used to generate the phase-locked reference is shown in Fig. 7. The prefilter provided voltage reduction and filtering any harmonics higher than the fundamental electrical frequency. The zero-crossing detector generated a pulse

at this frequency, which was reduced by the integer ratio, and used to generate a saw tooth at the lower frequency. Since a saw tooth waveform has both even and odd harmonics, all frequency multiples of the firing pulse were generated in the reference circuit.

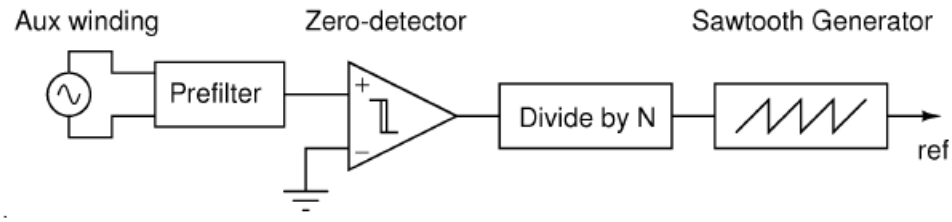

Fig. 7 – Pseudo-schematic of reference generation circuit.

The F×LMS controller used was constrained to specific control bandwidths in order to limit the amount of power required to drive the source speaker. The primary contributions to the total A-weighted SPL coming from the machine were grouped primary in a band from 50–500 Hz, and another from approximately 1 100–1 500 Hz. This can be seen in the "control off" plots of the Fig. 3. The contributions from 1 1 00–1 500 Hz were well within the frequency range of using passive treatment, so only the range less than 500 Hz was chosen for the active control bandwidth.

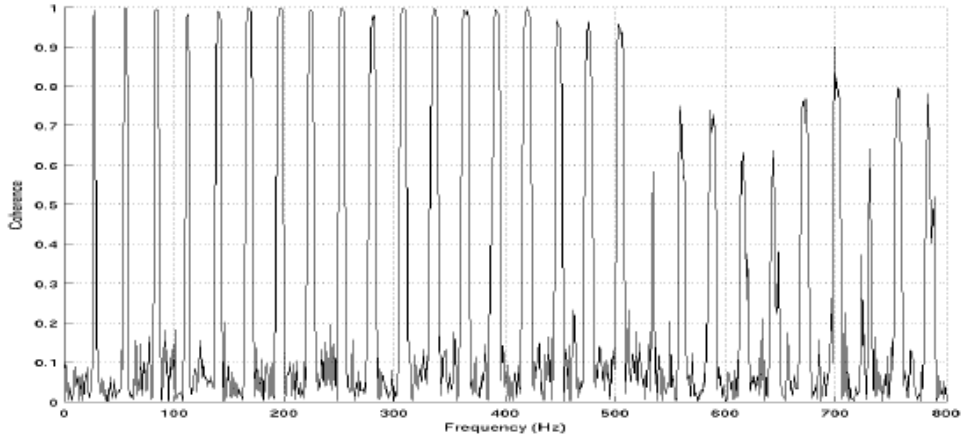

Fig. 8 – Measured coherence between reference signal and far field microphone.

Using the reference circuit, the F×LMS algorithm was implemented in a PC with dedicated real-time data acquisition boards and a DSP coprocessor card. Analog filters were configured on the reference, error and output channels to limit the control bandwidth. A total of 256 coefficients were used with a sample rate of

4 096 Hz. For most of the tests, a Single-Input, Single-Output control configuration was used.

6. EXPERIMENTAL RESULTS

The purpose of these reported tests was to demonstrate the potential of ANC for low frequency noise reduction. Future work will consider integrating the active speaker into the enclosure structure. The performance of the passive and active treatments was measured on the generator via a microphone located on each of its four sides at a distance of 3m from the machine center. The generator was run outside in a semi-reverberant location. The microphone near the operator panel was chosen as the error microphone for the active control.

The performance of the 0–500 Hz bandwidth active control at the error microphone can be seen in Fig. 9. The back and red lines show the narrowband spectrum of the error microphone with and without the active control running. The blue and magenta lines show a commutative integral of the same data. The cumulative integral indicates the overall sound level summed from 0 Hz to the frequency of interest. The total broadband performance is the difference between the two curves at the maximum plotted frequency. What this shows is that although the harmonics between 0–500 Hz are reduced between 15–30 dB, after the remaining spectrum from 500–2 000 Hz the aggregate reduction is only 3–4 dB. This shows the need to include the passive treatment. The overall reduction is limited by the set of tones centered on 1 400 Hz.

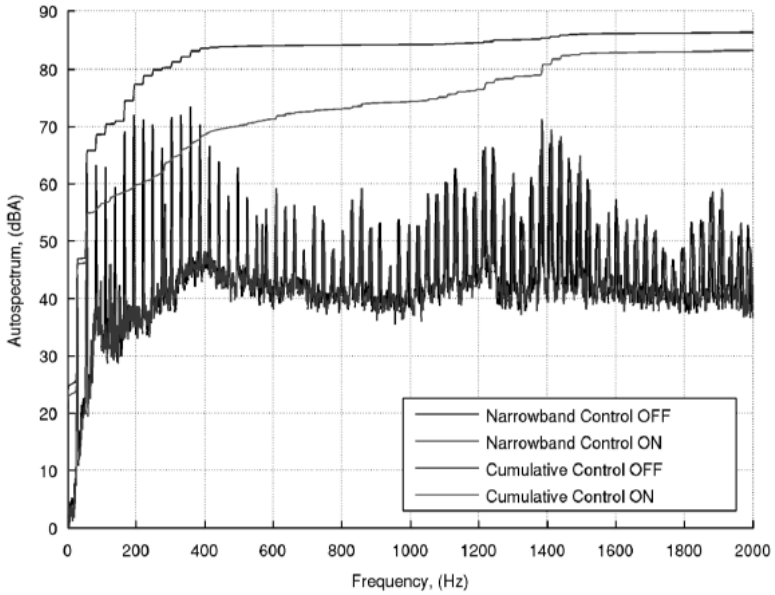

Fig. 9 – Narrowband and cumutative integral spectral plot of error signal with and without active control.

For the advanced passive control, two different configurations were studied. The first consisted of stiffeners on acoustically "hot" panels and additional poro elastic located in the housing interior. Fig. 10 shows the operator side microphone baseline case, as well as the two passive cases and two cases of the aforementioned passive treatment with active control turned on. A significant reduction in radiated sound level can be seen in the 700–3 000 Hz frequency hands with the addition of the absorbing material on the bottom of the unit near the drainage holes indicating that they leaked significant sound energy at higher frequencies. In addition, the active control can be seen from Fig. 10 to provide significant reduction in the targeted band of either 0–500 Hz or 100–500 Hz. The second considered an addition of absorbing material to areas located just below drainage holes on the bottom of the machine casing.

Fig. 11 shows the performance at all four microphone locations summed together to give an indication of global sound radiation from the machine.

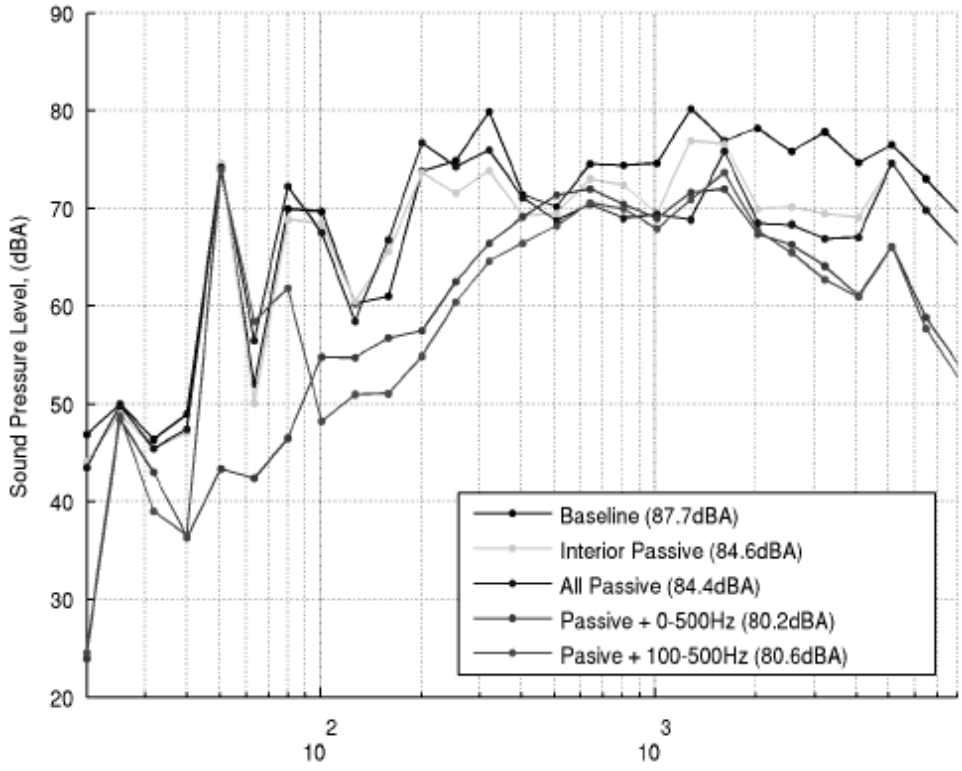

Fig. 10 – Treatment and active control performance
(error microphone in 1/3 rd octave bands).

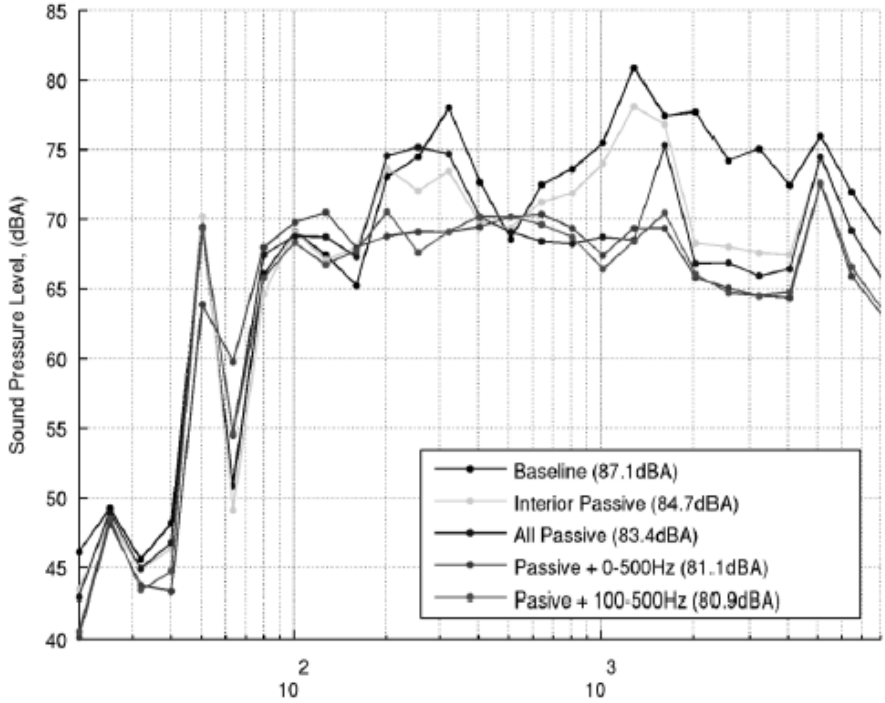

Fig. 11 – Treatment and active control performance
(mean of four monitor microphonees in 1/3 rd octave bands).

7. CONCLUSIONS

This paper describes the full scale implementation of passive and active noise control on a portable diesel generator. Although the unit was already designed with sound reduction in mind, a noise audit using coherence and phase array imaging techniques was employed to locate remaining dominant noise sources. Active control using F×LMS was implemented on the low-frequency noise using a custom hybrid analog /digital reference circuit phase-locked to the generator output. High-frequency passive treatment included panel stiffening and absorbing material.

Received June 7, 2011

REFERENCES

1. FULLER, C.R., ELLIOTT, S.J., NELSON P.A., *Active Control of Vibration*, Academic Press, London, 1997.
2. KUO, S.M., MORGAN, D.R., *Active noise control: a tutorial review*, Proceedings of the IEEE, **87**, *6*, pp. 943-973, 1999.

3. HOGAN, Michael C., LATSHAW Gary L., *The relationship between highway planning and urision specialty conference*, May 21-23, 1973, Chicago, Illinois, organized by American Society of Civil Engineers, Urban Transportation Division.
4. ROSEN, S., OLIN, P., *Hearing Loss and Coronary Heart Disease*, Archives of Otolaryngology, **82**, pp. 236-243, 1965.
5. FIELD, James M., *Effect of personal and situational variables upon noise annoyance in residential areas*, Journal of the Acoustical Society of America, **93**, *5*, pp. 2753-2763, 1993.
6. KRYTER, Karl D., *The Effects of Noise on Man*, Academic Press, 1985.
7. ROSENHALL, U., PEDERSEN, K., SVANBORG, A., *Presbycusis and noise-induced hearing loss*, Ear Hear, **11**, *4*, pp. 257-263, 1990.
8. MILIUS, S., *High Volume, Low Fidelity: Birds are less faithful as sounds blare*, Science News, **172**, p. 116, 2007.